

Lyapunov-based Adaptive Transformer (LyAT) for Control of Stochastic Nonlinear Systems

Saiedeh Akbari*, Xuehui Shen*, Wenqian Xue*, Jordan C. Insinger*, and Warren E. Dixon*

Abstract—This paper presents a novel Lyapunov-based Adaptive Transformer (LyAT) controller for stochastic nonlinear systems. While transformers have shown promise in various control applications due to sequential modeling through self-attention mechanisms, they have not been used within adaptive control architectures that provide stability guarantees. Existing transformer-based approaches for control rely on offline training with fixed weights, resulting in open-loop implementations that lack real-time adaptation capabilities and stability assurances. To address these limitations, a continuous LyAT controller is developed that adaptively estimates drift and diffusion uncertainties in stochastic dynamical systems without requiring offline pre-training. A key innovation is the analytically derived adaptation law constructed from a Lyapunov-based stability analysis, which enables real-time weight updates while guaranteeing probabilistic uniform ultimate boundedness of tracking and parameter estimation errors. Experimental validation on a quadrotor demonstrates the performance of the developed controller.

Index Terms—transformers, neural networks, Lyapunov methods, adaptive control, nonlinear control systems

I. INTRODUCTION

Deep learning has emerged as a powerful tool for nonlinear control due to its universal function approximation capabilities [1], and has been used as means of identification and control for dynamics with unstructured uncertainties [2]–[8]. Transformers are deep learning architectures that have revolutionized sequential modeling through self-attention mechanisms, making them well-suited for control problems requiring long-term temporal reasoning [9]. Transformers offer significant advantages for controlling stochastic nonlinear systems due to their ability to handle uncertainty through attention mechanisms and efficiently process complex sequential data in parallel. Unlike traditional neural network architectures, transformers allow for simultaneous processing of entire sequences and therefore provide global context awareness, which is crucial in control applications where past states significantly influence current control decisions.

The architectural evolution from recurrent neural networks (RNNs) to long short-term memory (LSTM) networks to transformers indicates the progression in modeling temporal

dependencies (e.g., [10] and [11]). RNNs suffer from vanishing gradients that limit long-term dependency capture [12], while LSTMs improve retention through gating mechanisms but compress history into fixed-size hidden states, potentially losing critical information [13]. Transformers overcome these limitations through attention mechanisms that maintain direct access to all previous states and dynamically weight historical information based on system performance without computationally expensive recurrent loops [9].

Transformers are the primary architecture used in natural language processing (NLP) in the recent years, but their application to control has been limited. Since their introduction [9], there have been some efforts to apply transformers in control systems, including PID controller integration [14], reinforcement learning [15], and specialized applications such as quantum feedback control and power flow adjustment (cf., [16] and [17]). However, to the best of the authors' knowledge, transformers have not been formalized and integrated within an adaptive control architecture.

Most existing deep learning approaches for control rely on offline training using sampled input-output datasets (e.g., [18, Sec. 6.6] and [19]–[21]). These architectures are typically applied as feedforward terms with fixed weights that cannot be updated in real-time. Recent breakthroughs develop Lyapunov-based update laws that adjust neural network weights in real-time through analytical update laws constructed from a stability analysis [22]–[28]. Specifically, the weights are updated using analytically-derived laws designed through Lyapunov-based stability analysis that enables real-time adaptation of the parameters of the architecture without requiring offline pre-training [22], [23]. While Lyapunov-based Deep RNNs, LSTMs, and Deep LSTMs have been developed for deterministic systems, despite the superior ability of transformers to capture long-term dependencies through attention mechanisms, they have not been integrated within adaptive control frameworks with stability guarantees.

The control of stochastic systems presents additional analytical challenges but offers considerable advantages since modeling uncertainty as stochastic processes makes control designs less conservative than assuming worst-case bounds [29]. Neural network-based learning methods are particularly valuable for nonlinear stochastic systems due to their black-box approximation capabilities [30]–[36]. However, despite considerable performance improvements from Lyapunov-based learning methods, their application to deep learning architectures for stochastic systems remains very limited (cf., [26] and [37]).

*Department of Mechanical and Aerospace Engineering, University of Florida, USA Email: {akbaris, xuehuishen, w.xue, jordan.insinger, wdixon}@ufl.edu.

This research is supported in part by AFRL project FA8651-24-1-0018, AFOSR grant FA9550-19-1-0169, and AFOSR grant FA9550-21-1-0157. Any opinions, findings, and conclusions or recommendations expressed in this material are those of the author(s) and do not necessarily reflect the views of the sponsoring agencies.

Addressing these gaps, this work develops the first Lyapunov-based Adaptive Transformer (LyAT) controller for stochastic nonlinear systems. Adapting transformers from NLP applications to real-time control requires overcoming substantial architectural and theoretical challenges. The key contributions of the developed result include the following.:

- 1) Transformer architecture design for real-time adaptive control: Unlike NLP applications where inputs (tokens) are straightforward, control applications require strategic input selection to assist with control objectives and system stabilization. In this paper, where the objective is tracking a desired trajectory, the inputs are designed as states, desired trajectories, and tracking errors to enable the attention mechanism to focus on tracking performance. The architecture is modified by removing embedding layers and modifying projection matrices to accommodate asymmetric encoder-decoder dimensions. The encoder processes rich state and trajectory information while the decoder focuses on uncertainty estimation (drift and diffusion), with the cross-attention mechanism handling the dimension mismatch through its projection matrices. This new asymmetric design is particularly beneficial for control applications because it eliminates the constraint that encoder and decoder inputs must be the same size, allowing each to be optimized for its specific role. The resulting continuous LyAT controller adaptively estimates drift and diffusion uncertainties which are then used in the control law.
- 2) Lyapunov-based parameter adaptation without pre-training: Existing transformers require massive offline training and training data which is mostly not available or feasible to attain in control applications. In this paper, an analytical parameter update law is constructed from Lyapunov-based stability analysis enabling real-time weight adjustment across all transformer layers using only streaming system feedback. This eliminates offline training while providing provable performance certificates.
- 3) Unified architecture and stability analysis: A constructive Lyapunov-based analysis guarantees probabilistic uniform ultimate boundedness of tracking and parameter estimation errors. This work streamlines the stability analysis approach of [26] by employing a single neural network architecture to simultaneously compensate for all uncertain terms arising from both drift and diffusion dynamics. In contrast to the more traditional feedforward DNN architecture in the prior work in [26] that required multiple DNNs for separate uncertainty components, in addition to the unique adaptive transformer design, the developed method in this paper also includes a unified network that incorporates the tracking error into its input, rather than solely the system states. This design enables efficient adaptation across all uncertainty channels while reducing computational and memory overhead.
- 4) Experimental results: Experimental validation on a Freefly Astro quadrotor tracking a figure-8 trajectory

demonstrates rapid convergence from initial conditions with a root mean square (RMS) tracking error of 0.2175 meters over 240 seconds of flight, demonstrating efficacy of the theoretical stability guarantees and practical applicability of the developed approach.

II. PROBLEM FORMULATION

A. Notation

An identity matrix of size n is denoted by $I_n \in \mathbb{R}^{n \times n}$. The right pseudo-inverse of full row rank matrix $A \in \mathbb{R}^{n \times m}$ is denoted by A^+ , where $A^+ \triangleq A^\top (AA^\top)^{-1}$. A zero matrix with dimension of $p \times q$ is denoted as $\mathbf{0}_{p \times q}$. The rectified linear unit (ReLU) activation function is denoted as $\sigma_{\text{ReLU}}(x) \triangleq \max(0, x)$. Given some functions f and g and some $w \in \mathbb{R}$, the notation $f(w) = \mathcal{O}^m(g(w))$ means that $\|f(w)\| \leq M \|g(w)\|^m$ for all $w \geq w_0$, where $M \in \mathbb{R}_{>0}$ and $w_0 \in \mathbb{R}$ denote constants. The vectorization operator is denoted by $\text{vec}(\cdot)$, i.e., given $A \triangleq [a_{i,j}] \in \mathbb{R}^{n \times m}$, $\text{vec}(A) \triangleq [a_{1,1}, \dots, a_{n,1}, \dots, a_{1,m}, \dots, a_{n,m}]^\top$. Given input $z \in \mathbb{R}^k$ and tunable constant parameters $\gamma, \beta \in \mathbb{R}$, the layer norm function $\text{LayerNorm}(z, \gamma, \beta) \in \mathbb{R}^k$ is defined as $\text{LayerNorm}(z, \gamma, \beta) \triangleq \frac{\gamma(z - \mu_z)}{\sigma_z} + \beta$, where $\mu_z \triangleq \frac{1}{k} \sum_{i=1}^k z_i$ and $\sigma_z \triangleq \sqrt{\frac{1}{k} \sum_{i=1}^k (z_i - \mu_z)^2}$. Given an input $Z \triangleq [z_1, \dots, z_q]^\top \in \mathbb{R}^{q \times k}$, the LayerNorm is applied row-wise, that is, the i^{th} row $z_i \in \mathbb{R}^k$ is normalized independently as $\text{LayerNorm}(z_i, \gamma, \beta)$, resulting in an output $\text{LayerNorm}(Z, \gamma, \beta) \in \mathbb{R}^{q \times k}$. Given an input $z \triangleq \{z_1, \dots, z_k\} \in \mathbb{R}^k$, the softmax function is defined as $\text{softmax}(z) \triangleq \frac{\exp(z_j)}{\sum_{j=1}^k \exp(z_j)}$. Given the input Z , the softmax function is applied row-wise, that is, the i^{th} row $z_i \in \mathbb{R}^k$ is independently normalized as $\text{softmax}(z_i)$, resulting in an output matrix $\text{softmax}(Z) \in \mathbb{R}^{k \times q}$. For a square matrix $A \in \mathbb{R}^{n \times n}$, the trace operator is defined as $\text{tr}(A) = \sum_{i=1}^n a_{i,i}$, where $a_{i,i}$ represents the element of the i^{th} row on the i^{th} column. From [38, Chapter 2, Eq. 13], the trace to vector property

$$\text{tr}(A^\top B) = \text{vec}(A)^\top \text{vec}(B) \quad (1)$$

holds for matrices A and B . From [38, Chapter 1, Eq. 25],

$$\text{tr}(ABC) = \text{tr}(BCA) = \text{tr}(CAB). \quad (2)$$

Additionally, if A and B are positive semi-definite matrices, then

$$\text{tr}(AB) \leq \text{tr}(A) \text{tr}(B). \quad (3)$$

Given a function $h : \mathbb{R}^n \rightarrow \mathbb{R}^n$, the notation $\lim_{a \rightarrow b^-} h(a)$ denotes the left-hand limit of h at b . The p -norm is denoted by $\|\cdot\|_p$, where the subscript is suppressed when $p = 2$. The Frobenius norm is denoted by $\|\cdot\|_F \triangleq \|\text{vec}(\cdot)\|$. For a bounded function $f : \mathbb{R}_{\geq 0} \rightarrow \mathbb{R}^{n \times m}$, $\|f\|_{F_\infty} \triangleq \sup_{t \in \mathbb{R}_{>0}} \|f\|_F$.

The space of k -times differentiable functions is denoted by C^k , and a C^∞ -smooth function is an infinitely differentiable

function. In the filtered probability space of $(\Omega, \mathbb{F}, \mathbb{F}_t, P)$, Ω represents the event space, \mathbb{F} denotes a σ -algebra of the subsets of Ω and represents the event space, \mathbb{F}_t is a complete filtration given by the family of σ -algebras up to time t , i.e., $\mathbb{F}_S : \mathbb{F}_S \subseteq \mathbb{F}_t \quad \forall t \in [0, t]$, and P is a probability measure, where the filtration is complete in the sense that it includes all events with probability measure zero (see [39]). Consider a probability space of (Ω, \mathbb{F}, P) . Therefore, for any events $A, B \in \mathbb{F}$ such that $A \subseteq B$, the monotonicity property states that [40, eq. 2.5]

$$P(A) \leq P(B). \quad (4)$$

Consider a stochastic differential equation (SDE) as $dx = f(x)dt + g(x, t)d\omega$. Then, for some function $V \in \mathcal{C}^2$ associated with this SDE, let the infinitesimal generator \mathcal{L} of the function $V(x)$ be defined as [41, eq. 4.12]

$$\mathcal{L}V \triangleq \frac{\partial V}{\partial x}f(x) + \frac{1}{2}\text{tr}\left(g(x, t)^\top \frac{\partial^2 V}{\partial x^2}g(x, t)\right). \quad (5)$$

Lemma 1. ([26, Lemma 1]) For the Ito process $z \in \mathbb{R}^n$ and function V , assume

(A1) V is non-negative, $V(0) = 0$, and $V \in \mathcal{C}^2$ over the open and connected set $Q_m \triangleq \{z : V(z) < m\}$, where $m \in \mathbb{R}_{>0}$ is a bounding constant,

(A2) $z(t)$ is a continuous strong Markov process defined until at least some $\tau' > \tau_m = \inf\{t : z(t) \notin Q_m\}$ with probability one.¹

If $\mathcal{L}V(z) \leq -k_1V(z) + k_2$ in Q_m for $k_1, k_2 > 0$, then for $\ell \leq m$, $z(t)$ is uniformly ultimately bounded in probability (UUB-p) with the probability

$$P\left(\sup_{t \leq s < \infty} V(z(s)) \geq \ell\right) \leq \frac{1}{m}V(z(0)) + \frac{1}{\ell}V(z(0))\exp(-k_1t) + \frac{k_2}{k_1\ell}. \quad (6)$$

B. System Dynamics and Control Objective

Consider the system dynamics modeled as

$$dx = (f(x) + g_1(x)u(t))dt + g_2(x)\Sigma(t)d\omega, \quad (7)$$

where $x : \mathbb{R}_{\geq 0} \rightarrow \mathbb{R}^n$ denotes the state, $u : \mathbb{R}_{\geq 0} \rightarrow \mathbb{R}^m$ denotes the control input, $f : \mathbb{R}^n \rightarrow \mathbb{R}^n$ denotes an unknown continuous drift vector, and $g_1 : \mathbb{R}^n \rightarrow \mathbb{R}^{n \times m}$ denotes the known full-row rank and bounded control effectiveness matrix.² Additionally, in (7), $g_2 : \mathbb{R}^n \rightarrow \mathbb{R}^{n \times s}$ denotes the unknown continuous diffusion matrix, $\Sigma : \mathbb{R}_{\geq 0} \rightarrow \mathbb{R}^{s \times s}$ denotes the symmetric Borel-measurable covariance matrix, and $\omega \in \mathbb{R}^s$ denotes the s -dimensional independent standard Wiener process defined on the complete filtered probability space $(\Omega, \mathbb{F}, \mathbb{F}_t, P)$.

The control objective is to design a LyAT-based controller that ensures the states track a user-defined desired trajectory,

¹This assumption guarantees the existence of the process up to τ' with probability one.

²The control development in [42] can be used to account for an uncertain, linearly parametrizable control effectiveness matrix g .

$x_d : \mathbb{R}_{\geq 0} \rightarrow \mathbb{R}^n$. To quantify the tracking objective, the tracking error, $e : \mathbb{R}_{\geq 0} \rightarrow \mathbb{R}^n$, is defined as

$$e \triangleq x - x_d. \quad (8)$$

Assumption 1. The desired trajectory x_d is designed to be sufficiently smooth, i.e., $\|x_d(t)\| \leq \bar{x}_d$ and $\|\dot{x}_d(t)\| \leq \dot{\bar{x}}_d$ for all $t \in \mathbb{R}_{\geq 0}$, where $\bar{x}_d, \dot{\bar{x}}_d \in \mathbb{R}_{>0}$ are known constants.

To adapt to the uncertainties in the diffusion matrix in the subsequent stability analysis, Taylor's expansion theorem is applied to the vectorized diffusion matrix g_2 , yielding

$$\begin{aligned} \text{vec}(g_2(x)) &= \text{vec}(g_2(x_d)) + \frac{\partial \text{vec}(g_2(x_d))}{\partial x_d}(x - x_d) \\ &\quad + \mathcal{O}(\|x - x_d\|^2) \\ &= \text{vec}(g_2(x_d)) + \frac{\partial \text{vec}(g_2(x_d))}{\partial x_d}e + \mathcal{O}(\|e\|^2) \\ &= G_2(e, x_d)e + \text{vec}(g_2(x_d)), \end{aligned} \quad (9)$$

where $G_2 : \mathbb{R}^n \times \mathbb{R}^n \rightarrow \mathbb{R}^{ns \times n}$ is a \mathcal{C}^∞ function, and $\text{vec}(g_2(x_d))$ is upper-bounded as $\|\text{vec}(g_2(x_d))\| \leq \bar{g}$, where $\bar{g} \in \mathbb{R}_{>0}$ is unknown.

III. TRANSFORMER NEURAL NETWORK ARCHITECTURE

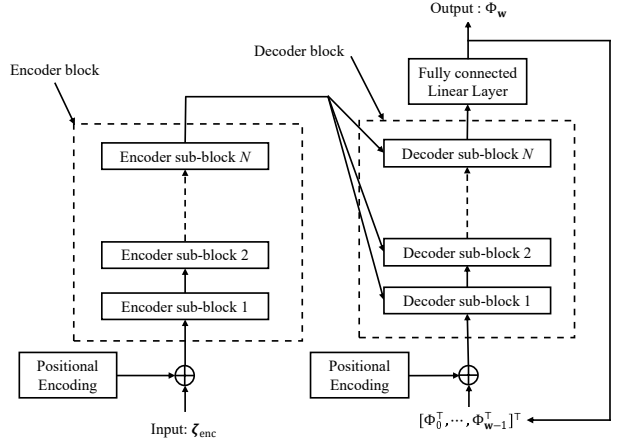


Fig. 1. An overview of the encoder-decoder transformer architecture. The transformer architecture consists of N encoder layers and N decoder layers.

A LyAT, denoted as $\Phi : \mathbb{R}^{3n\tau} \times \mathbb{R}^p \rightarrow \mathbb{R}^n$, is developed to compensate for the drift and diffusion uncertainties, $\mathcal{F} : \mathbb{R}^{3n} \rightarrow \mathbb{R}^n$, that appear in the subsequent stability analysis as $\mathcal{F}(x) \triangleq f(x) + \frac{1}{2}e\|\Sigma\Sigma^\top\|_{F_\infty}\text{tr}\{G_2^\top(e, x_d)G_2(e, x_d)\} + \|\Sigma\Sigma^\top\|_{F_\infty}G_2^\top(e, x_d)\text{vec}(g_2(x_d))$, where $x \triangleq [x^\top, x_d^\top, e^\top]^\top \in \mathbb{R}^{3n}$ is the current state information. The transformer has an encoder-decoder structure as illustrated in Figures 1 and 2. To form the network's input, the data is structured into sequences. The input to the encoder is a sequence of the last $\tau \in \mathbb{Z}_{>0}$ steps, i.e., $\zeta_{\text{enc}} \triangleq [x_1^\top, x_{d,1}^\top, e_1^\top, \dots, x_\tau^\top, x_{d,\tau}^\top, e_\tau^\top]^\top \in \mathbb{R}^{3n\tau}$. The

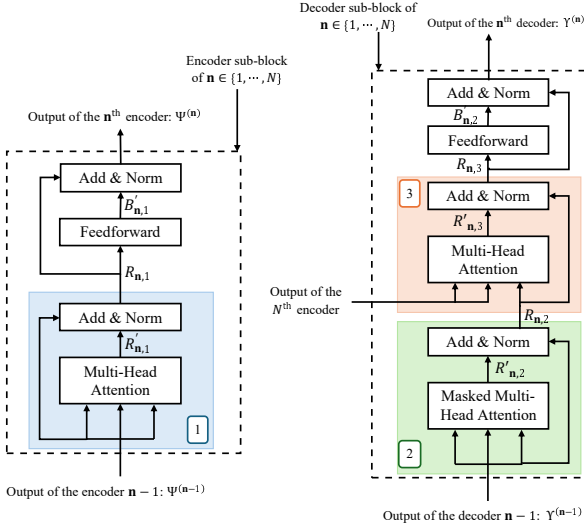


Fig. 2. A modular schematic of each attention-based encoder and decoder in a transformer architecture. Across these blocks, there are three key attention mechanisms, illustrated as 1, 2, and 3: self-attention, masked self-attention, and cross-attention, respectively.

input to the decoder is the last τ estimates of the LyAT output, $[\Phi_0^\top, \dots, \Phi_{\tau-1}^\top]^\top \in \mathbb{R}^{n\tau}$.

Remark 1. During the initial transient phase before τ historical values are available, the encoder and decoder inputs are populated with initialization values (e.g., zeros, inputs from offline training if available, or random inputs) that are sequentially updated with the actual state measurements and network outputs.

Remark 2. The encoder input ζ_{enc} , while mathematically represented as a concatenated vector, is structured and processed as a sequence of τ positions for the transformer architecture. Specifically, each position $i \in \{1, 2, \dots, \tau\}$ contains the concatenated state information $[x_i^\top, x_{d,i}^\top, e_i^\top]^\top \in \mathbb{R}^{3n}$, enabling the multi-head attention mechanism to capture temporal dependencies across the historical window.

Remark 3. The encoder focuses on tracking performance by processing a window of size τ containing historical state information ζ_{enc} to capture temporal patterns in system dynamics and tracking behavior. The decoder focuses on function approximation by receiving a window of the previous τ transformer output estimates, $\Phi_0, \dots, \Phi_{\tau-1}$, and using cross-attention to query relevant patterns from the encoder. Through cross-attention, the decoder queries the encoder's tracking-oriented representations to refine its uncertainty estimates. This architecture enables the transformer to condition its drift and diffusion compensation on both historical tracking performance and its own previous approximations.

The encoder block, consisting of N identical encoder sub-blocks, maps the input sequence to a sequence of continuous representations, $\Psi^{(N)} \in \mathbb{R}^{3n\tau}$. The latent sequence

³The input to the encoder can be viewed as a window of x_i , for all $i \in \{1, 2, \dots, \tau\}$, as $\zeta_{\text{enc}} = [x_1^\top, \dots, x_\tau^\top]^\top$, where x_τ for notational simplicity is written as $x_\tau = x$.

$\Psi^{(N)}$ is then utilized by the decoder stack's cross-attention mechanism, also consisting of N identical decoder sub-blocks. The decoder also processes the feedback sequence $[\Phi_0^\top, \dots, \Phi_{\tau-1}^\top]^\top \in \mathbb{R}^{n\tau}$ and maps that to the final output of the N -layer decoder, $\Upsilon^{(N)} \in \mathbb{R}^{n\tau}$, which is then used to compute the transformer estimate in continuous time. Each encoder and decoder block internally uses multi-head attention mechanisms and position-wise feedforward networks.

Remark 4. In the traditional Transformer architecture (cf., [9]), both the input to the multi-head attention in the encoder block and the input to the masked multi-head attention are first processed through an input embedding layer. This embedding mechanism is essential in language models where the inputs are typically tokens or words that need to be converted to numerical signals. However, in this paper, the LyAT is applied to estimate the drift and diffusion uncertainties of a stochastic dynamical system. Since the inputs in this context are already numerical values, the input embedding layer is not implemented.

A. Positional Encoding

The encoder and decoder blocks both contain a positional encoding to provide a sense of temporal or spatial order to the input data. Therefore, the inputs of the encoder and the decoder blocks are first fed into a positional encoding mechanism. For the encoder, the positional encoding for each $i \in \{1, \dots, \tau\}$ is defined as [9]

$$\begin{aligned} \text{PE}_{(i-1,2j)}^{\text{enc}} &= \sin\left(\frac{i-1}{10000^{\frac{2j}{3n}}}\right), \\ \text{PE}_{(i-1,2j+1)}^{\text{enc}} &= \cos\left(\frac{i-1}{10000^{\frac{2j}{3n}}}\right), \end{aligned} \quad (10)$$

where $j \in \{0, 1, \dots, \frac{3n-1}{2}\}$. For each $i \in \{1, \dots, \tau\}$ in the sequence, positional encoding vectors of the encoder $\text{PE}_{i-1}^{\text{enc}} \triangleq [\text{PE}_{(i-1,0)}^{\text{enc}}, \text{PE}_{(i-1,1)}^{\text{enc}}, \dots, \text{PE}_{(i-1,3n-1)}^{\text{enc}}]^\top$ are stacked as $\mathcal{U}_{\text{enc}} \triangleq [\text{PE}_0^{\text{enc}\top}, \text{PE}_1^{\text{enc}\top}, \dots, \text{PE}_{\tau-1}^{\text{enc}\top}]^\top \in \mathbb{R}^{3n\tau}$. For the decoder, the positional encoding for each $i \in \{1, \dots, \tau\}$ is defined as

$$\begin{aligned} \text{PE}_{(i-1,2j)}^{\text{dec}} &= \sin\left(\frac{i-1}{10000^{\frac{2j}{n}}}\right), \\ \text{PE}_{(i-1,2j+1)}^{\text{dec}} &= \cos\left(\frac{i-1}{10000^{\frac{2j}{n}}}\right), \end{aligned} \quad (11)$$

where $j \in \{0, 1, \dots, \frac{n-1}{2}\}$. For each $i \in \{0, \dots, \tau-1\}$ in the sequence, positional encoding vectors of the decoder $\text{PE}_{i-1}^{\text{dec}} \triangleq [\text{PE}_{(i-1,0)}^{\text{dec}}, \text{PE}_{(i-1,1)}^{\text{dec}}, \dots, \text{PE}_{(i-1,n-1)}^{\text{dec}}]^\top$ are stacked as $\mathcal{U}_{\text{dec}} \triangleq [\text{PE}_0^{\text{dec}\top}, \text{PE}_1^{\text{dec}\top}, \dots, \text{PE}_{\tau-1}^{\text{dec}\top}]^\top \in \mathbb{R}^{n\tau}$.

B. Attention Mechanism

The attention mechanism is designed as a mapping of a query and a set of key-value pairs to an output, where the query, keys, and values are all vector outputs of fully-connected layers. The output of the attention mechanism

is computed as a weighted sum of the values. The weight associated with each value is computed using a compatibility function of the query with the corresponding key. This weighted sum is computed over $H \in \mathbb{Z}_{>0}$ heads, resulting in a multi-head attention mechanism. The multi-head design allows the transformer to perform attention multiple times in parallel [9]. Since each head has its own set of query, keys, and values, the model is able to focus on different parts of the input simultaneously and learn different aspects of the data that may not be captured by a single attention head. A mathematical model of the multihead attention mechanism is subsequently provided.

An attention mechanism computes its output from two sources of input. One source, denoted $A_{n,\ell}(t) \triangleq \left[\left(a_{\ell,1}^{(n)} \right)^\top, \dots, \left(a_{\ell,\tau}^{(n)} \right)^\top \right]^\top$, provides the input for the key and value vectors, and the other source, denoted as $C_{n,\ell}(t) \triangleq \left[\left(c_{\ell,1}^{(n)} \right)^\top, \dots, \left(c_{\ell,\tau}^{(n)} \right)^\top \right]^\top$, provides the input for the query, for $n \in \{1, 2, \dots, N\}$ and $\ell \in \{1, 2, 3\}$.⁴ The output for each of the attention mechanism of each layer, denoted as $R_{n,1} \in \mathbb{R}^{3n\tau}, R_{n,2}, R_{n,3} \in \mathbb{R}^{n\tau}$, is defined as

$$R_{n,\ell}(t) \triangleq \text{LayerNorm}(C_{n,\ell}(t) + R'_{n,\ell}(t), \gamma_{n,\ell}, \beta_{n,\ell}), \quad (12)$$

for $\ell \in \{1, 2, 3\}$ and $n \in \{1, 2, \dots, N\}$, where $\gamma_{n,\ell}, \beta_{n,\ell} \in \mathbb{R}_{>0}$ are user-selected constants. The output of the Multi-Head Attention for each layer are denoted as $R'_{n,1} \in \mathbb{R}^{3n\tau}, R'_{n,2}, R'_{n,3} \in \mathbb{R}^{n\tau}$ and defined as

$$R'_{n,\ell}(t) \triangleq \left(\left[\left(H_{\ell,1}^{(n)} \right)^\top, \left(H_{\ell,2}^{(n)} \right)^\top, \dots, \left(H_{\ell,H}^{(n)} \right)^\top \right] \mathcal{W}_\ell^{(n)} \right)^\top,$$

where $\mathcal{W}_1^{(n)} \in \mathbb{R}^{3n \times 3n\tau}, \mathcal{W}_2^{(n)}, \mathcal{W}_3^{(n)} \in \mathbb{R}^{n \times n\tau}$ denote the matrices of multi-head weights. These multi-head matrices can be vectorized as $\theta_W = \left[\text{vec}(\mathcal{W}_1^{(1)})^\top, \dots, \text{vec}(\mathcal{W}_1^{(N)})^\top, \text{vec}(\mathcal{W}_2^{(1)})^\top, \dots, \text{vec}(\mathcal{W}_2^{(N)})^\top, \text{vec}(\mathcal{W}_3^{(1)})^\top, \dots, \text{vec}(\mathcal{W}_3^{(N)})^\top \right]^\top \in \mathbb{R}^{11n^2N\tau}$. For each head of the multihead attention block $h \in \{1, 2, \dots, H\}$, and $n \in \{1, 2, \dots, N\}$,

$$H_{\ell,h}^{(n)}(t) \triangleq \begin{cases} \text{softmax} \left(\frac{Q_{\ell,h}^{(n)} (K_{\ell,h}^{(n)})^\top}{\sqrt{d_k}} \right) V_{\ell,h}^{(n)}, & \ell = 1, 3, \\ \text{softmax} \left(\frac{Q_{\ell,h}^{(n)} (K_{\ell,h}^{(n)})^\top}{\sqrt{d_k}} + M_n \right) V_{\ell,h}^{(n)}, & \ell = 2, \end{cases} \quad (13)$$

where $M_n \in \mathbb{R}^{d_k^{\text{enc}} \times d_k^{\text{enc}}}$ denotes the mask, $d_k^{\text{enc}} = \frac{3n}{H}$, and $d_k^{\text{dec}} = \frac{n}{H}$.⁵ The query $(Q_{1,h}^{(n)} : \mathbb{R}^{3n\tau} \rightarrow \mathbb{R}^{d_k^{\text{enc}}}, Q_{2,h}^{(n)}, Q_{3,h}^{(n)} : \mathbb{R}^{n\tau} \rightarrow \mathbb{R}^{d_k^{\text{dec}}})$

⁴For the self-attention mechanism in the encoder (Attention Mechanism 1) of the first layer, $A_{1,1}(t) = C_{1,1}(t) = \zeta_{\text{enc}}(t) + \mathcal{U}_{\text{enc}}(t)$. For the masked multi-head attention mechanism in the decoder (Attention Mechanism 2) of the first layer, $A_{1,2}(t) = C_{1,2}(t) = [\Phi_0^\top, \dots, \Phi_{\tau-1}^\top]^\top + \mathcal{U}_{\text{dec}}$. For the cross-attention mechanism in the decoder (Attention Mechanism 3) of the first layer, $A_{1,3}(t) = \Psi^{(N)}(t)$ and $C_{1,3}(t) = R_{1,2}(t)$.

⁵Note, n is divisible by H .

$\mathbb{R}^{n\tau} \rightarrow \mathbb{R}^{d_k^{\text{dec}}})$, key $(K_{1,h}^{(n)} : \mathbb{R}^{3n\tau} \rightarrow \mathbb{R}^{d_k^{\text{enc}}}, K_{2,h}^{(n)} : \mathbb{R}^{n\tau} \rightarrow \mathbb{R}^{d_k^{\text{dec}}}, K_{3,h}^{(n)} : \mathbb{R}^{3n\tau} \rightarrow \mathbb{R}^{d_k^{\text{dec}}})$, and value $(V_{1,h}^{(n)} : \mathbb{R}^{3n\tau} \rightarrow \mathbb{R}^{d_k^{\text{dec}}}, V_{2,h}^{(n)} : \mathbb{R}^{n\tau} \rightarrow \mathbb{R}^{d_k^{\text{dec}}}, V_{3,h}^{(n)} : \mathbb{R}^{3n\tau} \rightarrow \mathbb{R}^{d_k^{\text{dec}}})$ are modeled as

$$Q_{\ell,h}^{(n)} = \left(\mathcal{W}_{\ell,h}^{(n)} \right)^\top \mathbf{c}_{n,\ell}(t), \quad (14)$$

$$K_{\ell,h}^{(n)} = \left(\mathbb{W}_{\ell,h}^{(n)} \right)^\top \mathbf{a}_{n,\ell}(t), \quad (15)$$

$$V_{\ell,h}^{(n)} = \left(\mathbf{W}_{\ell,h}^{(n)} \right)^\top \mathbf{a}_{n,\ell}(t), \quad (16)$$

for $\ell \in \{1, 2, 3\}, h \in \{1, \dots, H\}$, and $n \in \{1, 2, \dots, N\}$. The matrices $\mathcal{W}_{1,h}^{(n)} \in \mathbb{R}^{3n\tau \times d_k^{\text{enc}}}, \mathcal{W}_{2,h}^{(n)}, \mathcal{W}_{3,h}^{(n)} \in \mathbb{R}^{n\tau \times d_k^{\text{dec}}}$ denote the h^{th} query weights of the multihead of the n^{th} layer, and these query weights are vectorized as $\theta_W \triangleq \left[\text{vec}(\mathcal{W}_{1,1}^{(1)})^\top, \dots, \text{vec}(\mathcal{W}_{1,H}^{(1)})^\top, \dots, \text{vec}(\mathcal{W}_{1,1}^{(N)})^\top, \dots, \text{vec}(\mathcal{W}_{1,H}^{(N)})^\top, \dots, \text{vec}(\mathcal{W}_{3,1}^{(1)})^\top, \dots, \text{vec}(\mathcal{W}_{3,H}^{(1)})^\top \right]^\top \in \mathbb{R}^{11Nn^2\tau}$. The matrices $\mathbb{W}_{1,h}^{(n)} \in \mathbb{R}^{3n\tau \times d_k^{\text{enc}}}, \mathbb{W}_{2,h}^{(n)} \in \mathbb{R}^{n\tau \times d_k^{\text{dec}}}, \mathbb{W}_{3,h}^{(n)} \in \mathbb{R}^{3n\tau \times d_k^{\text{dec}}}$, denote the weights associated with the h^{th} key of the multihead of the n^{th} layer, and these key weights are vectorized as $\theta_W \triangleq \left[\text{vec}(\mathbb{W}_{1,1}^{(1)})^\top, \dots, \text{vec}(\mathbb{W}_{1,H}^{(1)})^\top, \dots, \text{vec}(\mathbb{W}_{1,1}^{(N)})^\top, \dots, \text{vec}(\mathbb{W}_{1,H}^{(N)})^\top, \dots, \text{vec}(\mathbb{W}_{3,1}^{(1)})^\top, \dots, \text{vec}(\mathbb{W}_{3,H}^{(1)})^\top \right]^\top \in \mathbb{R}^{13Nn^2\tau}$. The matrices $\mathbf{W}_{1,h}^{(n)} \in \mathbb{R}^{3n\tau \times d_k^{\text{enc}}}, \mathbf{W}_{2,h}^{(n)} \in \mathbb{R}^{n\tau \times d_k^{\text{dec}}}, \mathbf{W}_{3,h}^{(n)} \in \mathbb{R}^{3n\tau \times d_k^{\text{dec}}}$ denotes the weights associated with the h^{th} value of the multihead of the n^{th} layer, and these matrices are vectorized as $\theta_W \triangleq \left[\text{vec}(\mathbf{W}_{1,1}^{(1)})^\top, \dots, \text{vec}(\mathbf{W}_{1,H}^{(1)})^\top, \dots, \text{vec}(\mathbf{W}_{3,1}^{(1)})^\top, \dots, \text{vec}(\mathbf{W}_{3,H}^{(1)})^\top \right]^\top \in \mathbb{R}^{13Nn^2\tau}$. For the Masked Multihead Attention ($\ell = 2$), the elements of the matrix M_n are calculated as

$$M_{i,j}^{(n)} = \begin{cases} 0, & \text{for } i \geq j, \\ -\infty, & \text{for } i < j. \end{cases} \quad (17)$$

C. Encoder Block

In addition to the attention mechanism, each of the N encoder blocks is composed of two main sub-layers, a multi-head self-attention mechanism, followed by a fully connected feedforward network. The output of the multi-head attention sub-layer for the n^{th} encoder block, $R_{n,\ell}$, serves as the input

to the feedforward sub-layer. The output of each feedforward sub-layer is denoted as $B'_{n,1} \in \mathbb{R}^{3n\tau}$ and calculated as

$$B'_{n,1} \triangleq W_{f2}^{(n)\top} \sigma_{\text{ReLU}} \left(W_{f1}^{(n)\top} R_{n,1}(t) \right), \quad (18)$$

where $W_{f1}^{(n)} \in \mathbb{R}^{3n\tau \times d_f}$ and $W_{f2}^{(n)} \in \mathbb{R}^{d_f \times 3n\tau}$ denote the feedforward encoder weights, and $d_f \in \mathbb{Z}_{>0}$ denotes the size of the hidden layer of the feedforward network. The encoder feedforward weight matrices are vectorized as $\theta_{f1} = \left[\text{vec} \left(W_{f1}^{(1)} \right)^\top, \dots, \text{vec} \left(W_{f1}^{(N)} \right)^\top \right]^\top \in \mathbb{R}^{3nN\tau d_f}$ and $\theta_{f2} = \left[\text{vec} \left(W_{f2}^{(1)} \right)^\top, \dots, \text{vec} \left(W_{f2}^{(N)} \right)^\top \right]^\top \in \mathbb{R}^{3nN\tau d_f}$. The output of the n^{th} encoder block is denoted as $\Psi^{(n)} \in \mathbb{R}^{3n\tau}$ and defined as

$$\Psi^{(n)}(t) = \text{LayerNorm} \left(R_{n,1}(t) + B'_{n,1}, \gamma_f^{(n)}, \beta_f^{(n)} \right), \quad (19)$$

where $\gamma_f^{(n)}, \beta_f^{(n)} \in \mathbb{R}_{>0}$ denote user-selected constants.

D. Decoder Block

Each of the N identical decoder blocks is composed of three main sub-layers, a masked multi-head self-attention, a multi-head cross-attention mechanism that incorporates the N^{th} encoder's output, and a fully connected feedforward network. The output of the cross-attention sub-layer for the n^{th} decoder block, $R_{n,3}$, serves as the input to the feedforward network. The output of the feedforward network is denoted as $B'_{n,2} \in \mathbb{R}^{n\tau}$ and modeled as

$$B'_{n,2} \triangleq W_{F2}^{(n)\top} \sigma_{\text{ReLU}} \left(W_{F1}^{(n)\top} R_{n,3}(t) \right), \quad (20)$$

where $W_{F1}^{(n)} \in \mathbb{R}^{n\tau \times d_f}$ and $W_{F2}^{(n)} \in \mathbb{R}^{d_f \times n\tau}$ denote the feed-forward decoder weights. The decoder feedforward weights are defined as $\theta_{F1} = \left[\text{vec} \left(W_{F1}^{(1)} \right)^\top, \dots, \text{vec} \left(W_{F1}^{(N)} \right)^\top \right]^\top \in \mathbb{R}^{Nn\tau d_f}$ and $\theta_{F2} = \left[\text{vec} \left(W_{F2}^{(1)} \right)^\top, \dots, \text{vec} \left(W_{F2}^{(N)} \right)^\top \right]^\top \in \mathbb{R}^{Nn\tau d_f}$. The output of the n^{th} encoder block is denoted as $\Upsilon^{(n)} \in \mathbb{R}^{n\tau}$ and defined as

$$\Upsilon^{(n)}(t) = \text{LayerNorm} \left(R_{n,3} + B'_{n,2}, \gamma_F^{(n)}, \beta_F^{(n)} \right), \quad (21)$$

where $\gamma_F^{(n)}, \beta_F^{(n)} \in \mathbb{R}_{>0}$ denote user-selected constants.

E. LyAT Output

Using the output of the decoder block, the LyAT output is denoted as $\Phi(\zeta_{\text{enc}}, \theta) \in \mathbb{R}^n$ and defined as

$$\Phi(\zeta_{\text{enc}}, \theta) \triangleq W_o^\top \sigma_{\text{ReLU}} \left(\Upsilon^{(n)} \right), \quad (22)$$

where $W_o \in \mathbb{R}^{n\tau \times n}$ denotes the output weight matrix. The stacked matrix of all the weights in the LyAT architecture is denoted as $\theta \in \mathbb{R}^p$ and defined as

$$\theta = \left[\theta_{\mathcal{W}}^\top, \theta_{\mathcal{W}}^\top, \theta_{\mathcal{W}}^\top, \theta_{\mathcal{W}}^\top, \theta_{f1}^\top, \theta_{f2}^\top, \theta_{F1}^\top, \theta_{F2}^\top, \text{vec}(W_o)^\top \right]^\top,$$

where the dimension p is quantified as $p \triangleq 48Nn^2\tau + 8Nn\tau d_f + n^2\tau$.

Recall, the output of the LyAT is used to compensate for the drift and diffusion uncertainties, $\mathcal{F} : \mathbb{R}^{3n} \rightarrow \mathbb{R}^n$. The function $\mathcal{F}(X)$ can be written as a function of the encoder input as $\mathcal{F}(X) = \mathcal{G}(\zeta_{\text{enc}})$ where $\mathcal{G}(\zeta_{\text{enc}})$ can be approximated using the universal function approximation as [43]

$$\mathcal{G}(\zeta_{\text{enc}}) = \Phi(\zeta_{\text{enc}}, \theta^*) + \varepsilon(\zeta_{\text{enc}}).$$

Since $\mathcal{F}(X) = \mathcal{G}(\zeta_{\text{enc}})$,

$$\mathcal{F}(X) = \Phi(\zeta_{\text{enc}}, \theta^*) + \varepsilon(\zeta_{\text{enc}}), \quad (23)$$

where $\varepsilon(\zeta_{\text{enc}}) : \mathbb{R}^{3n\tau} \rightarrow \mathbb{R}^n$ denotes an unknown function representing the reconstruction error that is bounded by an unknown $\bar{\varepsilon} \in \mathbb{R}_{>0}$ as

$$\sup_{x \in \Omega} \|\varepsilon(x)\| \leq \bar{\varepsilon}. \quad (24)$$

The approximation objective is to determine optimal estimates of θ such that $\zeta_{\text{enc}} \mapsto \Phi(\zeta_{\text{enc}}, \hat{\theta})$ approximates $X \mapsto \mathcal{F}(X)$ with minimal error for any $X \in \Omega$, where $\hat{\theta}$ denote the adaptive parameter estimates of the ideal weights θ^* . Let $\Omega \subset \mathbb{R}^p$ denote a user-selected compact and convex parameter search space with a smooth boundary, satisfying $0_p \in \text{int}(\Omega)$. Additionally, define $\bar{\theta} \triangleq \max_{\theta \in \Omega} \|\theta\|$ to be a bound on the user-selected search space.⁶

F. Weight Adaptation Law

The parameter estimation error is defined as

$$\tilde{\theta} \triangleq \theta^* - \hat{\theta}. \quad (25)$$

Through the subsequent stochastic Lyapunov stability analysis, the LyAT parameter update law is designed as

$$\dot{\hat{\theta}} \triangleq \text{proj} \left(\Gamma \Phi'^\top \left(\zeta_{\text{enc}}, \hat{\theta} \right) e - \Gamma \sigma \hat{\theta} \right), \quad (26)$$

where $\Gamma \in \mathbb{R}^{p \times p}$ denotes a user-selected positive-definite gain matrix, $\sigma \in \mathbb{R}_{>0}$ denote a user-defined forgetting factor, $\text{proj}(\cdot)$ denotes a smooth projection operator defined in [44, eq. (7)-(11)], which is used to ensure that $\hat{\theta}$ is bounded as $\|\hat{\theta}\| \leq \bar{\theta}$, and $\Phi'(\zeta_{\text{enc}}, \hat{\theta}) \triangleq \frac{\partial \Phi(\zeta_{\text{enc}}, \hat{\theta})}{\partial \theta}$.

To facilitate the subsequent stability analysis, a first-order Taylor approximation (cf., [23] and [45]) is used to state

$$\Phi(\zeta_{\text{enc}}, \theta^*) - \Phi(\zeta_{\text{enc}}, \hat{\theta}) = \Phi'(\zeta_{\text{enc}}, \hat{\theta}) \tilde{\theta} + \mathcal{R}(\zeta_{\text{enc}}, \tilde{\theta}), \quad (27)$$

where $\mathcal{R} : \mathbb{R}^{3n\tau} \times \mathbb{R}^p \rightarrow \mathbb{R}^n$ denotes Lagrange remainder term. The Lagrange remainder in (27) is unknown; however, the following lemma provides a polynomial bound for the term.

Lemma 2. *There exists a polynomial function $\rho_0 : \mathbb{R}_{\geq 0} \rightarrow \mathbb{R}_{\geq 0}$ of the form $\rho_0(\|x\|) = a_2 \|x\|^2 + a_1 \|x\| + a_0$ with some known constants $a_0, a_1, a_2 \in \mathbb{R}_{>0}$ such that the*

⁶For more information about using a bounded search space for $\hat{\theta}$ and uniqueness, see [27].

Lagrange remainder term can be bounded as $\|\mathcal{R}(x, \tilde{\theta})\| \leq \rho_0(\|x\|) \|\tilde{\theta}\|^2$ [46, Thm. 1].

IV. CONTROL DESIGN

To compensate for the uncertainties that appear in the subsequent closed-loop error system, the LyAT is incorporated into a controller designed as

$$u(t) \triangleq g_1^+(x) \left(\dot{x}_d - k_e e - \Phi(\zeta_{\text{enc}}, \hat{\theta}) \right), \quad (28)$$

where $k_e \in \mathbb{R}_{>0}$ denotes a user-defined control gain. Taking the differential of the tracking error in (8) and substituting (7) and (28), and canceling the cross terms yields the closed-loop tracking error

$$de = \left(f(x) - k_e e - \Phi(\zeta_{\text{enc}}, \hat{\theta}) \right) dt + g_2(x) \Sigma(t) d\omega. \quad (29)$$

Let $z : \mathbb{R}_{\geq 0} \rightarrow \mathbb{R}^{n+p}$ denote the concatenated error defined as $z \triangleq [e^\top, \hat{\theta}^\top]^\top$. By taking the differential of the concatenated error z and using (29), (25), and the chain rule, dz is obtained as $dz = [de^\top, \dot{\hat{\theta}}^\top dt]^\top$. Substituting (29) and (26) into dz yields the closed-loop error system in the form of a stochastic differential equation as

$$dz = \mathbf{F}(z) dt + \mathbf{G}(z, t) d\omega, \quad (30)$$

where $\mathbf{G}(z, t) \triangleq \left[(g_2(x) \Sigma(t))^\top, \mathbf{0}_{s \times p}^\top \right]^\top$ and

$$\mathbf{F} \triangleq \begin{bmatrix} f(x) - k_e e - \Phi(\zeta_{\text{enc}}, \hat{\theta}) \\ -\text{proj}(\Gamma \Phi'^\top(\zeta_{\text{enc}}, \hat{\theta}) e - \Gamma \sigma \hat{\theta}) \end{bmatrix}.$$

V. STABILITY ANALYSIS

Consider the Lyapunov function candidate $V_L : \mathbb{R}^{n+p} \rightarrow \mathbb{R}_{\geq 0}$ defined as

$$V_L(z) \triangleq \frac{1}{2} e^\top e + \frac{1}{2} \tilde{\theta}^\top \Gamma^{-1} \tilde{\theta}. \quad (31)$$

The Lyapunov function candidate in (31) can be bounded as

$$\alpha_1 \|z\|^2 \leq V_L(z) \leq \alpha_2 \|z\|^2, \quad (32)$$

where $\alpha_1 \triangleq \frac{1}{2} \min(1, \Gamma^{-1})$ and $\alpha_2 \triangleq \max(1, \Gamma^{-1})$.

For the universal function approximation property to hold, it is necessary to ensure $\zeta_{\text{enc}} \in \Omega$, for all $t \in \mathbb{R}_{\geq 0}$. To guarantee that $\zeta_{\text{enc}} \in \Omega$, the subsequent stability analysis contains z in a compact domain, for all $t \in \mathbb{R}_{\geq 0}$. Consider the compact domain $\mathcal{D} \triangleq \{\iota \in \mathbb{R}^{n+p} : \|\iota\| \leq \rho^{-1}(\mathbf{b}_0 - \mathbf{b}_2)\}$ in which z is supposed to lie for all time $t \in \mathbb{R}_{\geq 0}$, where $\mathbf{b}_0 \triangleq \min(\frac{k_e}{2}, \frac{\sigma}{2})$, $\mathbf{b}_2 \in \mathbb{R}_{>0}$ denotes the desired rate of convergence, and $\rho(\|z\|) \triangleq \rho_1(\|z\|) \|z\|$ is invertible. It follows that if $\|z\| \in \mathcal{D}$, then using (8), triangle inequality, and the bound on the desired trajectory yields

$$\begin{aligned} \|\mathbf{x}_i\| &\leq \|x_i\| + \|x_{d,i}\| + \|e_i\| \leq 2\|e_i\| + 2\|x_{d,i}\| \\ &\leq 2\rho^{-1}(\mathbf{b}_0 - \mathbf{b}_2) + 2\bar{x}_d, \end{aligned} \quad (33)$$

for all $i \in \{1, 2, \dots, \tau\}$. Since (33) holds for all $i \in \{1, 2, \dots, \tau\}$, then $\|\zeta_{\text{enc}}\| \leq \|\mathbf{x}_1\| + \dots + \|\mathbf{x}_\tau\| \leq 2\tau\rho^{-1}(\mathbf{b}_0 - \mathbf{b}_2) + 2\tau\bar{x}_d$. Therefore, select $\Omega \triangleq \{\iota \in \mathbb{R}^{3n\tau} : \|\iota\| \leq 2\tau\rho^{-1}(\mathbf{b}_0 - \mathbf{b}_2) + 2\tau\bar{x}_d\}$. Then, $z \in \mathcal{D}$ implies $\zeta_{\text{enc}} \in \Omega$. In the subsequent analysis, it is shown that if $z(0) \in \mathcal{S}$, then $z(t) \in \mathcal{D}$, for all $t \in \mathbb{R}_{\geq 0}$, where $\mathcal{S} \subset \mathcal{D}$ is defined

$$\mathcal{S} \triangleq \left\{ \iota \in \mathbb{R}^{n+p} : \|\iota\| \leq \sqrt{\frac{\alpha_1}{\alpha_2} (\rho^{-1}(\mathbf{b}_0 - \mathbf{b}_2))^2 - \frac{\mathbf{b}_1}{\mathbf{b}_2}} \right\}, \quad (34)$$

where $\mathbf{b}_1 \triangleq \frac{\varepsilon^2}{2k_e} + \frac{\sigma}{2} \tilde{\theta}^2 + \frac{1}{2} \|\Sigma\|_{F_\infty}^2 \bar{g}^2$. Note that the set \mathcal{S} exists when $\mathbf{b}_0 \geq \mathbf{b}_2 + \rho \left(\sqrt{\frac{\alpha_2}{\alpha_1} \frac{\mathbf{b}_1}{\mathbf{b}_2}} \right)$. Additionally, \mathcal{S} can be made arbitrarily large to include any initial condition $z(0)$ such that \mathbf{b}_0 satisfies the gain condition

$$\mathbf{b}_0 \geq \rho \left(\sqrt{\frac{\alpha_2}{\alpha_1} \|z\|^2 + \frac{\alpha_2}{\alpha_1} \frac{\mathbf{b}_1}{\mathbf{b}_2}} \right) + \mathbf{b}_2. \quad (35)$$

The gain condition in (35) is equivalent to stating the set \mathcal{S} is not a null set and contains the initial condition $z(0)$.

Since $\mathcal{S} \subset \mathcal{D}$, $z(0) \in \mathcal{S}$ implies $z(0) \in \mathring{\mathcal{D}}$ where $\mathring{\mathcal{D}}$ denotes the interior of \mathcal{D} . The solution $t \mapsto z(t)$ is assumed to be continuous on a time-interval $\mathcal{T} \triangleq [0, t_1]$ with probability one⁷ such that $z(t) \in \mathcal{D}$ for all $t \in \mathcal{T}$. It follows that $x(t) \in \Omega$, for all $t \in \mathcal{T}$, therefore the universal function approximation property holds over this time interval. In the subsequent stability analysis, the probabilistic convergence properties of the solutions are analyzed. Using Lemma 1 and to facilitate the analysis, the risk of z to escape \mathcal{D} is denoted as ϑ , which is defined as

$$\begin{aligned} \vartheta &\triangleq \frac{1}{\alpha_1 (\rho^{-1}(\mathbf{b}_0 - \mathbf{b}_2))^2} V_L(z(0)) \\ &\quad + \frac{1}{\lambda} V_L(z(0)) \exp \left(-\frac{\mathbf{b}_2}{\alpha_2} t \right) + \frac{\alpha_2 \mathbf{b}_1}{\lambda \mathbf{b}_2}, \end{aligned} \quad (36)$$

where $\lambda \in \left[\frac{\alpha_2 \mathbf{b}_1}{\mathbf{b}_2}, \alpha_1 (\rho^{-1}(\mathbf{b}_0 - \mathbf{b}_2))^2 \right]$.

Theorem 1. Consider the dynamical system in (7). Given the gain condition in (35), for any initial conditions of the process $z(0) \in \mathcal{S}$, the LyAT parameter adaptation law and the controller respectively given by (26) and (28) guarantee that the Ito process $z(t)$ is uniformly ultimately bounded in probability (UUB-p, c.f., [26, Def. 1]) in the sense that

$$P \left(\sup_{t \leq s < \infty} \|z(s)\| \leq \sqrt{\frac{\lambda}{\alpha_1}} \right) \geq 1 - \vartheta. \quad (37)$$

Proof: Taking the infinitesimal generator of the candidate Lyapunov function in (31) yields

$$\mathcal{L}V_L(z) = \frac{\partial V_L}{\partial z} \mathbf{F}(z) + \frac{1}{2} \text{tr} \left(\mathbf{G}^\top(z, t) \frac{\partial^2 V_L}{\partial z^2} \mathbf{G}(z, t) \right). \quad (38)$$

⁷This is a standard assumption in the analysis of stochastic systems (cf. [47, Page 36, Ass. (A2)]).

Substituting \mathbf{F} , \mathbf{G} , $\frac{\partial V_L}{\partial z}$, and $\frac{\partial^2 V_L}{\partial z^2}$ into (38) yields

$$\begin{aligned}\mathcal{L}V_L(z) &= e^\top \left(f(x) - k_e e - \Phi(\zeta_{\text{enc}}, \hat{\theta}) \right) \\ &\quad - \tilde{\theta}^\top \Gamma^{-1} \text{proj} \left(\Gamma \Phi'^\top (\zeta_{\text{enc}}, \hat{\theta}) e - \Gamma \sigma \hat{\theta} \right) \\ &\quad + \frac{1}{2} \text{tr} \left(\Sigma^\top(t) g_2^\top(x) g_2(x) \Sigma(t) \right).\end{aligned}\quad (39)$$

From [44, P2 in Thm. 1], $(\cdot) \leq \text{proj}(\cdot)$. Using this lower bound of $\text{proj}(\cdot)$ and applying the trace property from (2) on (39) yields

$$\begin{aligned}\mathcal{L}V_L &\leq e^\top \left(f(x) - k_e e - \Phi(\zeta_{\text{enc}}, \hat{\theta}) \right) - \tilde{\theta}^\top \Phi'^\top (\zeta_{\text{enc}}, \hat{\theta}) e \\ &\quad + \sigma \tilde{\theta}^\top \hat{\theta} + \frac{1}{2} \text{tr} \left(g_2^\top(x) g_2(x) \Sigma(t) \Sigma^\top(t) \right).\end{aligned}\quad (40)$$

Using the definition of the Frobenius norm on the term $\text{tr}(g_2^\top(x) g_2(x) \Sigma(t) \Sigma^\top(t))$ yields

$$\begin{aligned}\text{tr}(g_2^\top(x) g_2(x) \Sigma(t) \Sigma^\top(t)) &= \text{tr}(\Sigma^\top(t) g_2^\top(x) g_2(x) \Sigma(t)) \\ &= \text{tr}((g_2(x) \Sigma(t))^\top g_2(x) \Sigma(t)) \\ &= \|g_2(x) \Sigma(t)\|_F^2.\end{aligned}\quad (41)$$

Applying the Cauchy-Schwarz inequality [48, Page 189] to (41) yields

$$\begin{aligned}\|g_2(x) \Sigma(t)\|_F^2 &\leq \|g_2(x)\|_F^2 \|\Sigma(t)\|_F^2 \\ &= \text{tr}(g_2^\top(x) g_2(x)) \|\Sigma(t)\|_F^2.\end{aligned}\quad (42)$$

Using (3), (41), (42), and the fact that $\|\Sigma(t)\|_F^2 \leq \sup_{t \in \mathbb{R}_{\geq 0}} \|\Sigma(t)\|_F^2 \triangleq \|\Sigma\|_{F\infty}^2$, the term $\text{tr}(g_2^\top(x) g_2(x) \Sigma(t) \Sigma^\top(t))$ in (40) is upper bounded as

$$\text{tr}(g_2^\top(x) g_2(x) \Sigma(t) \Sigma^\top(t)) \leq \text{tr}(g_2^\top(x) g_2(x)) \|\Sigma\|_{F\infty}^2.\quad (43)$$

Thus, applying (43) to (40), applying the trace-to-vector property in (1) to $\text{tr}(g_2^\top g_2)$, and substituting (9) into (40) yields

$$\begin{aligned}\mathcal{L}V_L &\leq e^\top \left(f(x) - k_e e - \Phi(\zeta_{\text{enc}}, \hat{\theta}) \right) - \tilde{\theta}^\top \Phi'^\top (\zeta_{\text{enc}}, \hat{\theta}) e \\ &\quad + \sigma \tilde{\theta}^\top \hat{\theta} + \frac{1}{2} \|\Sigma\|_{F\infty}^2 \left(e^\top G_2^\top(e, x_d) G_2(e, x_d) e \right. \\ &\quad \left. + 2e^\top G_2^\top(e, x_d) \text{vec}(g_2(x_d)) \right. \\ &\quad \left. + \text{vec}(g_2(x_d))^\top \text{vec}(g_2(x_d)) \right).\end{aligned}\quad (44)$$

Since $e^\top G_2^\top(e, x_d) G_2(e, x_d) e = \text{tr}\{e^\top G_2^\top(e, x_d) G_2(e, x_d) e\}$, using (2) and (3) and upper-bounding $\text{vec}(g_2(x_d))$ as $\text{vec}(g_2(x_d)) \leq \|\text{vec}(g_2(x_d))\| \leq \bar{g}$, yields

$$\begin{aligned}\mathcal{L}V_L &\leq e^\top \left(f(x) - k_e e - \Phi(\zeta_{\text{enc}}, \hat{\theta}) \right) - \tilde{\theta}^\top \Phi'^\top (\zeta_{\text{enc}}, \hat{\theta}) e \\ &\quad + \sigma \tilde{\theta}^\top \hat{\theta} + \frac{1}{2} \|\Sigma\|_{F\infty}^2 e^\top \text{etr}\{G_2^\top(e, x_d) G_2(e, x_d)\} \\ &\quad + \|\Sigma\|_{F\infty}^2 e^\top G_2^\top(e, x_d) \text{vec}(g_2(x_d)) + \frac{1}{2} \|\Sigma\|_{F\infty}^2 \bar{g}^2.\end{aligned}\quad (45)$$

Applying the definition of \mathcal{F} and then using (23) yields

$$\begin{aligned}\mathcal{L}V_L &\leq e^\top \left(-k_e e + \Phi(\zeta_{\text{enc}}, \theta^*) - \Phi(\zeta_{\text{enc}}, \hat{\theta}) + \varepsilon(\zeta_{\text{enc}}) \right) \\ &\quad - \tilde{\theta}^\top \Phi'^\top (\zeta_{\text{enc}}, \hat{\theta}) e + \sigma \tilde{\theta}^\top \hat{\theta} + \frac{1}{2} \|\Sigma\|_{F\infty}^2 \bar{g}^2.\end{aligned}\quad (46)$$

Applying the Taylor series approximation in (27) on (46) and canceling cross terms yields

$$\mathcal{L}V_L \leq e^\top \left(-k_e e + \Delta(\zeta_{\text{enc}}, \tilde{\theta}) \right) + \sigma \tilde{\theta}^\top \hat{\theta} + \frac{1}{2} \|\Sigma\|_{F\infty}^2 \bar{g}^2,\quad (47)$$

where $\Delta : \mathbb{R}^{3n\tau} \times \mathbb{R}^p \rightarrow \mathbb{R}^n$ is defined as $\Delta(\zeta_{\text{enc}}, \tilde{\theta}) \triangleq \varepsilon(\zeta_{\text{enc}}) + \mathcal{R}(\zeta_{\text{enc}}, \tilde{\theta})$. By using (8), (24), Lemma 2, the triangle inequality, and boundedness of desired trajectory, the term $\Delta(\zeta_{\text{enc}}, \tilde{\theta})$ can be bounded as

$$\|\Delta(\zeta_{\text{enc}}, \tilde{\theta})\| \leq \bar{\varepsilon} + \rho_0 \left(2 \sum_{i=1}^{\tau} \|e_i\| + 2\tau \bar{x}_d \right) \|\tilde{\theta}\|^2,\quad (48)$$

for all $t \in \mathcal{T}$. Since ρ_0 is strictly increasing, the term $\rho_0(2 \sum_{i=1}^{\tau} \|e_i\| + 2\tau \bar{x}_d)$ can be upper-bounded as $\rho_0(2 \sum_{i=1}^{\tau} \|e_i\| + 2\tau \bar{x}_d) \leq \rho_0(2 \sum_{i=1}^{\tau} \|z_i\| + 2\tau \bar{x}_d)$. Using this upper bound and concatenated error definition, (48) is further upper-bounded as

$$\|\Delta(\zeta_{\text{enc}}, \tilde{\theta})\| \leq \bar{\varepsilon} + \rho_1(\|z_i\|) \|z\|^2,\quad (49)$$

where $\rho_1(\|z_i\|) = \rho_0(2 \sum_{i=1}^{\tau} \|z_i\| + 2\tau \bar{x}_d)$, for all $t \in \mathcal{T}$. Applying (49) and (25) to (47) yields

$$\begin{aligned}\mathcal{L}V_L &\leq -k_e \|e\|^2 + |e^\top| \bar{\varepsilon} + |e^\top| \rho_1(\|z_i\|) \|z\|^2 \\ &\quad - \sigma \|\tilde{\theta}\|^2 + \sigma \|\tilde{\theta}\| \|\theta^*\| + \frac{1}{2} \|\Sigma\|_{F\infty}^2 \bar{g}^2,\end{aligned}\quad (50)$$

for all $t \in \mathcal{T}$. Let $\rho(\|z_i\|) \triangleq \rho_1(\|z_i\|) \|z\|$. From (50), using the bound of θ^* and applying Young's inequality on $\bar{\varepsilon} \|e\|$ and $\sigma \bar{\theta} \|\tilde{\theta}\|$ yields

$$\mathcal{L}V_L \leq -(\mathbf{b}_0 - \rho(\|z_i\|)) \|z\|^2 + \mathbf{b}_1,\quad (51)$$

for all $t \in \mathcal{T}$. Based on the definition of \mathcal{D} , it follows that for each $i \in \{1, \dots, \tau\}$ that $\rho(\|z_i\|) \leq \mathbf{b}_0 - \mathbf{b}_2$. Therefore,

$$\mathcal{L}V_L \leq -\mathbf{b}_2 \|z\|^2 + \mathbf{b}_1,\quad (52)$$

for all $t \in \mathcal{T}$. Applying (32) to (52) yields

$$\mathcal{L}V_L \leq -\frac{\mathbf{b}_2}{\alpha_2} V_L + \mathbf{b}_1,\quad (53)$$

for all $t \in \mathcal{T}$.

Since $V_L(0) = 0$, $V_L \in \mathcal{C}^2$, and z is a continuous strong Markov process, based on (53), then [26, Lemma 1] can be invoked to state

$$P \left(\sup_{t \leq s \leq \infty} V_L(z(s)) \geq \lambda \right) \leq \vartheta,$$

which is equivalent to

$$P \left(\sup_{t \leq s \leq \infty} V_L(z(s)) < \lambda \right) \geq 1 - \vartheta,\quad (54)$$

for all $t \in \mathcal{T}$. From (32), $P\left(\sup_{t \leq s < \infty} \|z(s)\|^2 < \frac{\lambda}{\alpha_1}\right) \geq P\left(\sup_{t \leq s < \infty} V_L(z(s)) < \lambda\right)$. Therefore, using (54) and Lemma 1 yields (37), for all $t \in \mathcal{T}$. From (37) and [26, Def. 1], the solution $z(t)$ is UUB-p, for all $t \in \mathcal{T}$. ■

Remark 5. The tunable parameters such as k_e directly influences the parameters b_0 , b_1 , and b_2 , which in turn affect ρ^{-1} and the size of the initialization set. By making ρ^{-1} larger, the admissible range for λ can be increased. From (36), larger values of λ and ρ^{-1} result in smaller ϑ , thereby increasing the probability $1 - \vartheta$ that z remains bounded.

Let $S_1 \triangleq \left\{z : \|z(t)\| < \sqrt{\frac{\lambda}{\alpha_1}}\right\}$ and $S_2 \triangleq \left\{z : \|e(t)\| < \sqrt{\frac{\lambda}{\alpha_1}}\right\}$. Since $S_1 \subseteq S_2$, the monotonicity property in (4) yields $P\left(\sup_{t \leq s < \infty} \|e(s)\| \leq \sqrt{\frac{\lambda}{\alpha_1}}\right) \geq P\left(\sup_{t \leq s < \infty} \|z(s)\| \leq \sqrt{\frac{\lambda}{\alpha_1}}\right) \geq 1 - \vartheta$, for all $i \in \{1, 2, \dots, \tau\}$. Let $S_{3,i} \triangleq \left\{z : \|z_i\| < \sqrt{\frac{\lambda}{\alpha_1}}\right\}$, for all $i \in \{1, 2, \dots, \tau\}$. Since $S_1 \subseteq S_{3,i}$, the monotonicity property in (4) yields $P\left(\sup_{t \leq s < \infty} \|z_i\| \leq \sqrt{\frac{\lambda}{\alpha_1}}\right) \geq P\left(\sup_{t \leq s < \infty} \|z(s)\| \leq \sqrt{\frac{\lambda}{\alpha_1}}\right) \geq 1 - \vartheta$, for all $i \in \{1, 2, \dots, \tau\}$. Let $S_{4,i} \triangleq \left\{z : \|e_i\| < \sqrt{\frac{\lambda}{\alpha_1}}\right\}$, for all $i \in \{1, 2, \dots, \tau\}$. Since $S_{3,i} \subseteq S_{4,i}$, the monotonicity property in (4) yields $P\left(\sup_{t \leq s < \infty} \|e_i\| < \sqrt{\frac{\lambda}{\alpha_1}}\right) \geq P\left(\sup_{t \leq s < \infty} \|z_i\| < \sqrt{\frac{\lambda}{\alpha_1}}\right) \geq 1 - \vartheta$, for all $i \in \{1, 2, \dots, \tau\}$. Let $S_{5,i} \triangleq \left\{z : \|x_i\| < \sqrt{\frac{\lambda}{\alpha_1} + \bar{x}_d}\right\}$, for all $i \in \{1, 2, \dots, \tau\}$. Since $S_{4,i} \subseteq S_{5,i}$, the monotonicity property in (4) yields $P\left(\sup_{t \leq s < \infty} \|x_i\| < \sqrt{\frac{\lambda}{\alpha_1} + \bar{x}_d}\right) \geq P\left(\sup_{t \leq s < \infty} \|e_i\| < \sqrt{\frac{\lambda}{\alpha_1}}\right) \geq 1 - \vartheta$, for all $i \in \{1, 2, \dots, \tau\}$. Since x_1, \dots, x_τ are not independent of each other and $P\left(\sup_{t \leq s < \infty} \|x_i\| \leq \sqrt{\frac{\lambda}{\alpha_1}}\right) \geq 1 - \vartheta$, it can be stated that

$$\begin{aligned} P\left(\left\{\sup_{t \leq s < \infty} \|x_1\| \leq \sqrt{\frac{\lambda}{\alpha_1}}\right\} \cap \dots \cap \left\{\sup_{t \leq s < \infty} \|x_\tau\| \leq \sqrt{\frac{\lambda}{\alpha_1}}\right\}\right) \\ \geq \min_{i \in \{1, \dots, \tau\}} \left(P\left(\sup_{t \leq s < \infty} \|x_1\| \leq \sqrt{\frac{\lambda}{\alpha_1}}\right), \dots, \right. \\ \left. P\left(\sup_{t \leq s < \infty} \|x_\tau\| \leq \sqrt{\frac{\lambda}{\alpha_1}}\right) \right) \geq 1 - \vartheta. \end{aligned} \quad (55)$$

Since e_1, \dots, e_τ are not independent of each other and

$P\left(\sup_{t \leq s < \infty} \|e_i\| \leq \sqrt{\frac{\lambda}{\alpha_1}}\right) \geq 1 - \vartheta$, it can be stated that

$$\begin{aligned} P\left(\left\{\sup_{t \leq s < \infty} \|e_1\| \leq \sqrt{\frac{\lambda}{\alpha_1}}\right\} \cap \dots \cap \left\{\sup_{t \leq s < \infty} \|e_\tau\| \leq \sqrt{\frac{\lambda}{\alpha_1}}\right\}\right) \\ \geq \min_{i \in \{1, \dots, \tau\}} \left(P\left(\sup_{t \leq s < \infty} \|e_1\| \leq \sqrt{\frac{\lambda}{\alpha_1}}\right), \dots, \right. \\ \left. P\left(\sup_{t \leq s < \infty} \|e_\tau\| \leq \sqrt{\frac{\lambda}{\alpha_1}}\right) \right) \geq 1 - \vartheta. \end{aligned} \quad (56)$$

From the boundedness of x_d and using (55), (56), there exists a constant $\bar{\zeta}_{\text{enc}}$ such that $P\left(\sup_{t \leq s < \infty} \|\zeta_{\text{enc}}\| < \bar{\zeta}_{\text{enc}}\right) \geq 1 - \vartheta$.

Since $P\left(\sup_{t \leq s < \infty} \|\zeta_{\text{enc}}\| < \bar{\zeta}_{\text{enc}}\right) \geq 1 - \vartheta$ and $\|\hat{\theta}\| \leq \bar{\theta}$, and based on the smoothness of $\Phi(\zeta_{\text{enc}}, \hat{\theta})$, there exists a constant $\bar{\Phi} \in \mathbb{R}_{>0}$ such that $P\left(\sup_{t \leq s < \infty} \|\Phi(\zeta_{\text{enc}}, \hat{\theta}(s))\| \leq \bar{\Phi}\right) \geq 1 - \vartheta$. Since $P\left(\sup_{t \leq s < \infty} \|\Phi(\zeta_{\text{enc}}, \hat{\theta}(s))\| \leq \bar{\Phi}\right) \geq 1 - \vartheta$, $P\left(\sup_{t \leq s < \infty} \|e(s)\| < \sqrt{\frac{\lambda}{\alpha_1}}\right) \geq 1 - \vartheta$, and $\|x_d\| \leq \bar{x}_d$, using (28) yields $P\left(\sup_{t \leq s < \infty} \|u(s)\| \leq \bar{u}\right) \geq 1 - \vartheta$, for some constant $\bar{u} \in \mathbb{R}_{>0}$. Therefore, all implemented signals are bounded with probability of $1 - \vartheta$.

VI. EXPERIMENT

A. Experimental Testbed

To verify the efficacy of the proposed LyAT control method, a 4-minute experimental validation is performed on a Freefly Astro quadrotor at the University of Florida's Autonomy Park outdoor facility. The Freefly Astro is a professional-grade quadcopter with an unfolded diameter of 930 mm (1407 mm including propellers), powered by four Freefly 7010 motors with 21×7 inches carbon fiber reinforced nylon folding propellers. The aircraft has a maximum gross takeoff weight of 8700 g, and the flight controller is a Freefly custom-designed Skynode running Auterion Enterprise PX4 firmware.

Onboard state estimation is provided by the PX4 EKF2 fusion algorithm, which combines measurements from GPS (L1/L2 bands supporting GPS, GLONASS, Beidou, and Galileo), optical flow, lidar, and barometer sensors. This multi-sensor fusion provides global position, altitude above mean sea level (AMSL), velocity estimates, and height above ground.

The LyAT controller is implemented in Python using PyTorch and integrated into a ROS2 framework. The ROS2 control loop operates at 50 Hz, though computational demands of the transformer architecture result in control commands being transmitted to the flight controller at approximately 20 Hz. Velocity commands are communicated to the PX4 autopilot via the MAVROS package, which converts ROS2



Fig. 3. The Freefly Astro quadrotor (image courtesy of Freefly Systems, <https://freeflysystems.com/astro>).

topics to MAVLink protocol messages. A maximum velocity saturation of $VEL_{max} = 1.8$ m/s is enforced on all control commands to ensure safe operation within the experimental flight zone.

B. Experimental Settings

The quadrotor is set to autonomously track a figure-8 desired trajectory modeled as

$$x_d = \begin{bmatrix} a \sin(\omega t) \\ b \sin(2\omega t) \\ h \\ a\omega \cos(\omega t) \\ 2b\omega \cos(2\omega t) \\ 0 \end{bmatrix},$$

where the height is $h = 2.5$ m, the angular frequency is $\omega = 0.15$ rad/sec, $a = 7.5$ m, and $b = 3$ m. The initial conditions are as $x(0) = [0, 0, 2.5, 0, 0, 0]^\top$. The LyAT architecture is configured with $N = 1$ encoder and decoder layers, with all multi-head attention mechanisms (self-attention, cross-attention, and masked self-attention) utilizing $H = 3$ attention heads. The feedforward dimension is set to $d_f = 5$, and the historical window size is $\tau = 20$ data points. During the initial transient phase before $\tau = 20$ historical data points are available, the decoder input is populated with random Gaussian noise scaled by 0.1, which are sequentially replaced with actual network outputs as they become available. Similarly, the encoder input uses zero-padding for unavailable historical states. The LayerNorm parameters are $\gamma_f = \gamma_{1,1} = 0.8$, $\gamma_{1,2} = \gamma_{1,3} = \gamma_F = 0.7$, and $\beta_f = \beta_{1,1} = \beta_{1,2} = \beta_{1,3} = \beta_F = 0$. The transformer weights are initialized using Xavier uniform initialization with gain 0.01. The adaptation learning rate is selected as $\Gamma = 0.02I$, and the forgetting factor is set as $\sigma = 10^{-6}$. The parameter bound and the control gain are selected as $\bar{\theta} = 10$ and $k_e = 0.8$, respectively.

C. Results and Discussion

The RMS tracking error in Figure 4 exhibits an initial transient peaking at approximately 1.5 meters, which is due

to the initial condition error. After approximately 10 seconds, the error converges to a steady-state ultimate bound with typical amplitudes between 0.1 to 0.3 meters. The persistent oscillations are potentially attributed to environmental disturbances, sensor noise and bias, and uncertain dynamics. The RMS tracking error across the entire 240-second flight is 0.2175 meters. Notably, the error remains uniformly bounded throughout the experiment, validating the theoretical UUB-p guarantee from Theorem 1.

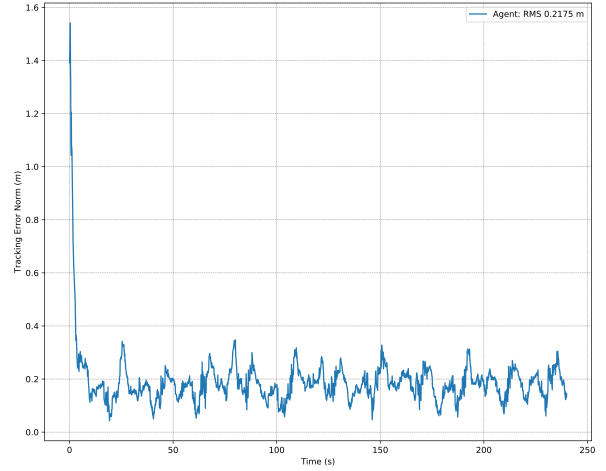


Fig. 4. Evolution of the RMS of the tracking error over 240 seconds.

The three-dimensional trajectory visualization in Figure 5 confirms the successful tracking of the figure-8 desired trajectory over 5.7 cycles. The quadrotor maintains close proximity to the desired trajectory throughout the maneuver, with slight deviations primarily visible during high-curvature portions at the figure-8 crossover points. The consistent altitude maintenance around 2.5m demonstrates effective compensation of both drift and diffusion uncertainties.

Figure 6 illustrates the control effort across all three spatial dimensions. To track the horizontal figure-8 motion, the X and Y channels show larger oscillations with respective peak magnitudes of approximately 1.2 m/s and 1 m/s, while the Z -channel requires minimal actuation of ± 0.2 m/s to maintain constant altitude. The initial control spike corresponds to the aggressive corrective action in response to the large initial tracking error. Following the transient, the control signals remain smooth and continuous, demonstrating the LyAT's ability to generate implementable commands without chattering or saturation.

These experimental results validate that the proposed LyAT controller successfully adapts to system uncertainties in real-time without requiring offline training, maintains bounded tracking error with RMS performance of 0.2175 meters, and generates smooth, implementable control signals suitable for physical quadrotor deployment. The rapid convergence and sustained performance over the full 240-second flight validate the effectiveness of the Lyapunov-based adaptation mechanism in compensating for both drift and diffusion uncertainties under real outdoor flight conditions.

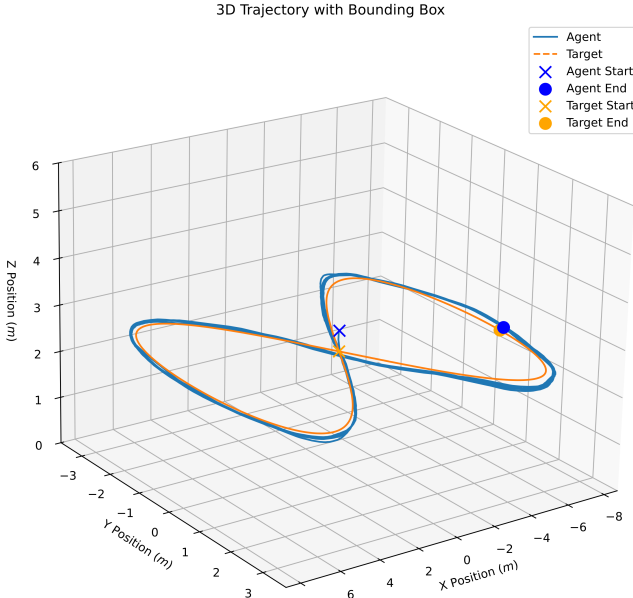


Fig. 5. Three-dimensional schematic of the trajectory tracking.

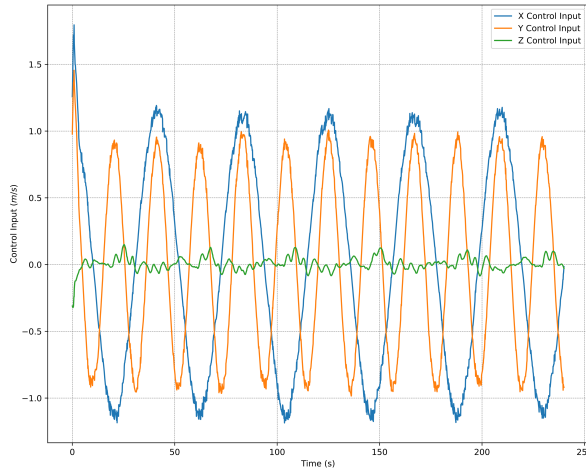


Fig. 6. Evolution of control input over 240 seconds.

VII. CONCLUSIONS

This paper presented a Lyapunov-based adaptive transformer controller for adaptive control of stochastic nonlinear systems with unstructured uncertainties. The developed transformer architecture features analytically-derived weight adaptation laws that enable real-time parameter updates without offline training requirements. A constructive Lyapunov-based stability analysis guarantees probabilistic uniform ultimate boundedness of tracking and parameter estimation errors. The unified neural network architecture simultaneously compensates for drift and diffusion uncertainties, significantly reducing computational complexity compared to prior methods requiring multiple separate networks [26]. Experimental validation on a Freefly Astro quadrotor tracking a figure-8

trajectory demonstrated rapid convergence to an ultimate and sustained performance with RMS tracking error of 0.2175 meters. The results confirm the LyAT's real-time adaptation capabilities and theoretical performance guarantees under real-world flight conditions with environmental disturbances.

REFERENCES

- [1] J. A. Anderson, *An introduction to neural networks*. MIT press, 1995.
- [2] M. O'Connell, G. Shi, X. Shi, K. Azizzadenesheli, A. Anandkumar, Y. Yue, and S.-J. Chung, "Neural-fly enables rapid learning for agile flight in strong winds," *Sci. Robotics*, vol. 7, no. 66, p. 6597, 2022.
- [3] G. Shi, X. Shi, M. O'Connell, R. Yu, K. Azizzadenesheli, A. Anandkumar, Y. Yue, and S.-J. Chung, "Neural lander: Stable drone landing control using learned dynamics," in *Proc. IEEE Int. Conf. Robot. Autom.*, pp. 9784–9790, 2019.
- [4] A. Punjani and P. Abbeel, "Deep learning helicopter dynamics models," in *Proc. IEEE Int. Conf. Robot. Autom.*, pp. 3223–3230, 2015.
- [5] S. Bansal, A. K. Akametalu, F. J. Jiang, F. Laine, and C. J. Tomlin, "Learning quadrotor dynamics using neural network for flight control," in *Proc. IEEE Conf. Decis. Control*, pp. 4653–4660, 2016.
- [6] Q. Li, J. Qian, Z. Zhu, X. Bao, M. K. Helwa, and A. P. Schoellig, "Deep neural networks for improved, impromptu trajectory tracking of quadrotors," in *Proc. IEEE Int. Conf. Robot. Autom.*, pp. 5183–5189, 2017.
- [7] S. Zhou, M. K. Helwa, and A. P. Schoellig, "Design of deep neural networks as add-on blocks for improving impromptu trajectory tracking," in *Proc. IEEE Conf. Decis. Cont.*, pp. 5201–5207, 2017.
- [8] P. Abbeel, A. Coates, and A. Y. Ng, "Autonomous helicopter aerobatics through apprenticeship learning," *Int. J. Robot. Research*, vol. 29, no. 13, pp. 1608–1639, 2010.
- [9] A. Vaswani, N. Shazeer, N. Parmar, J. Uszkoreit, L. Jones, A. N. Gomez, L. u. Kaiser, and I. Polosukhin, "Attention is all you need," in *Adv. Neural Inf. Process. Syst.* (I. Guyon, U. V. Luxburg, S. Bengio, H. Wallach, R. Fergus, S. Vishwanathan, and R. Garnett, eds.), vol. 30, 2017.
- [10] L. Medsker and L. C. Jain, *Recurrent neural networks: design and applications*. CRC press, 1999.
- [11] S. Hochreiter and J. Schmidhuber, "Long short-term memory," *Neural computation*, vol. 9, pp. 1735–80, 12 1997.
- [12] H. Salehinejad, S. Sankar, J. Barfett, E. Colak, and S. Valaee, "Recent advances in recurrent neural networks," *arXiv preprint arXiv:1801.01078*, 2017.
- [13] Y. Yu, X. Si, C. Hu, and J. Zhang, "A review of recurrent neural networks: Lstm cells and network architectures," *Neural Comput.*, vol. 31, no. 7, pp. 1235–1270, 2019.
- [14] T. M. Nguyen, C. A. Uribe, T. M. Nguyen, and R. Baraniuk, "Pidformer: Transformer meets control theory," in *41 Int. Conf. on Mach. Learning*, 2024.
- [15] D. Kim, J. D. Lee, H. Bang, and J. Bae, "Reinforcement learning-based fault-tolerant control for quadrotor with online transformer adaptation," *arXiv preprint arXiv:2505.08223*, 2025.
- [16] K. Chen, W. Luo, S. Liu, Y. Wei, Y. Zhou, Y. Qing, Q. Zhang, Y. Wang, J. Song, and M. Song, "Powerformer: A section-adaptive transformer for power flow adjustment," in *Proc. of the 31st ACM SIGKDD Conf. on Knowl. Discov. and Data Mining V. 1*, pp. 2204–2215, 2025.
- [17] P. Vaidhyanathan, F. Marquardt, M. T. Mitchison, and N. Ares, "Quantum feedback control with a transformer neural network architecture," *arXiv preprint arXiv:2411.19253*, 2024.
- [18] S. L. Brunton and J. N. Kutz, *Data-driven science and engineering: Machine learning, dynamical systems, and control*. Cambridge University Press, 2019.
- [19] K. Noda, H. Arie, Y. Suga, and T. Ogata, "Multimodal integration learning of robot behavior using deep neural networks," *Robotics & Auton. Syst.*, vol. 62, no. 6, pp. 721–736, 2014.
- [20] D. Sarikaya, J. J. Corso, and K. A. Guru, "Detection and localization of robotic tools in robot-assisted surgery videos using deep neural networks for region proposal and detection," *IEEE Trans. Med. Imaging*, vol. 36, no. 7, pp. 1542–1549, 2017.
- [21] H.-T. Nguyen and C. C. Cheah, "Analytic deep neural network-based robot control," *IEEE/ASME Trans. Mechatron.*, vol. 27, no. 4, pp. 2176–2184, 2022.

[22] O. Patil, D. Le, M. Greene, and W. E. Dixon, "Lyapunov-derived control and adaptive update laws for inner and outer layer weights of a deep neural network," *IEEE Control Syst Lett.*, vol. 6, pp. 1855–1860, 2022.

[23] O. S. Patil, D. M. Le, E. Griffis, and W. E. Dixon, "Deep residual neural network (ResNet)-based adaptive control: A Lyapunov-based approach," in *Proc. IEEE Conf. Decis. Control*, pp. 3487–3492, 2022.

[24] E. Griffis, O. Patil, W. Makumi, and W. E. Dixon, "Deep recurrent neural network-based observer for uncertain nonlinear systems," in *IFAC World Congr.*, pp. 6851–6856, 2023.

[25] S. Akbari, E. J. Griffis, O. S. Patil, and W. E. Dixon, "Lyapunov-based dropout deep neural network (Lb-DDNN) controller," *arXiv preprint arXiv:2310.19938*, 2023.

[26] S. Akbari, C. F. Nino, O. S. Patil, and W. E. Dixon, "Lyapunov-based deep neural networks for adaptive control of stochastic nonlinear systems," *arXiv preprint arXiv:2412.21095*, 2024.

[27] S. Akbari, O. S. Patil, and W. E. Dixon, "Lyla-therm: Lyapunov-based langevin adaptive thermodynamic neural network controller," *arXiv preprint arXiv:2508.14989*, 2025.

[28] X. Shen, E. Griffis, W. Wu, and W. E. Dixon, "Adaptive control via lyapunov-based deep long short-term memory networks," *IEEE Trans. Autom. Control*, to appear.

[29] P. R. Kumar and P. Varaiya, *Stochastic systems: Estimation, identification, and adaptive control*. SIAM, 2015.

[30] J. Li, W. Chen, J. Li, and Y. Fang, "Adaptive NN output-feedback stabilization for a class of stochastic nonlinear strict-feedback systems," *ISA Trans.*, vol. 48, no. 4, pp. 468–475, 2009.

[31] C. P. Chen, Y.-J. Liu, and G.-X. Wen, "Fuzzy neural network-based adaptive control for a class of uncertain nonlinear stochastic systems," *IEEE Trans. Cybern.*, vol. 44, no. 5, pp. 583–593, 2013.

[32] Z. Li, T. Li, G. Feng, R. Zhao, and Q. Shan, "Neural network-based adaptive control for pure-feedback stochastic nonlinear systems with time-varying delays and dead-zone input," *IEEE Trans. Syst., Man, & Cybern.: Syst.*, vol. 50, no. 12, pp. 5317–5329, 2018.

[33] H. Wang, P. X. Liu, J. Bao, X.-J. Xie, and S. Li, "Adaptive neural output-feedback decentralized control for large-scale nonlinear systems with stochastic disturbances," *IEEE Trans. Neural Netw. & Learning Syst.*, vol. 31, no. 3, pp. 972–983, 2019.

[34] L. Wang and C. P. Chen, "Reduced-order observer-based dynamic event-triggered adaptive NN control for stochastic nonlinear systems subject to unknown input saturation," *IEEE Trans. Neural Netw. & Learning Syst.*, vol. 32, no. 4, pp. 1678–1690, 2020.

[35] F. Wang, Z. You, Z. Liu, and C. P. Chen, "A fast finite-time neural network control of stochastic nonlinear systems," *IEEE Trans. Neural Netw. & Learning Syst.*, vol. 34, no. 10, pp. 7443–7452, 2022.

[36] W. Chen, L. Jiao, J. Li, and R. Li, "Adaptive NN backstepping output-feedback control for stochastic nonlinear strict-feedback systems with time-varying delays," *IEEE Trans. Syst., Man, & Cybern., Part B (Cybernetics)*, vol. 40, no. 3, pp. 939–950, 2009.

[37] J. Chen, J. Mei, J. Hu, and Z. Yang, "Deep neural networks-prescribed performance optimal control for stochastic nonlinear strict-feedback systems," *Neurocomp.*, p. 128633, 2024.

[38] J. R. Magnus and H. Neudecker, *Matrix differential calculus with applications in statistics and econometrics*. John Wiley & Sons, 2019.

[39] M. Lanchares and W. M. Haddad, "Stochastic thermodynamics: Dissipativity, accumulativity, energy storage and entropy production," *Philos. Trans. of the Royal Soc. A*, vol. 381, no. 2256, p. 20220284, 2023.

[40] P. Billingsley, *Probability and measure*. John Wiley & Sons, 2017.

[41] H. J. Kushner, *Stochastic stability and control*. ACADEMIC PRESS, INC., 1967.

[42] R. Sun, M. Greene, D. Le, Z. Bell, G. Chowdhary, and W. E. Dixon, "Lyapunov-based real-time and iterative adjustment of deep neural networks," *IEEE Control Syst. Lett.*, vol. 6, pp. 193–198, 2022.

[43] C. Yun, S. Bhojanapalli, A. S. Rawat, S. J. Reddi, and S. Kumar, "Are transformers universal approximators of sequence-to-sequence functions?," *arXiv preprint arXiv:1912.10077*, 2019.

[44] Z. Cai, M. S. de Queiroz, and D. M. Dawson, "A sufficiently smooth projection operator," *IEEE Trans. Autom. Control*, vol. 51, pp. 135–139, Jan. 2006.

[45] F. L. Lewis, A. Yesildirek, and K. Liu, "Multilayer neural-net robot controller with guaranteed tracking performance," *IEEE Trans. Neural Netw.*, vol. 7, no. 2, pp. 388–399, 1996.

[46] O. S. Patil, B. C. Fallin, C. F. Nino, R. G. Hart, and W. E. Dixon, "Bounds on deep neural network partial derivatives with respect to parameters," *arXiv preprint arXiv:2503.21007*, 2025.

[47] H. J. Kushner, *Introduction to Stochastic Control*. New York: Holt, Reinhart and Winston, 1971.

[48] S. Axler, *Linear algebra done right*. Springer Nature, 2024.